ChemPubSoc Europe

DOI: 10.1002/ejic.201800168

EurJIC European Journal of Inorganic Chemistry

Full Paper

Redox-Active Pincer Ligands

CLUSTER ISSUE

Nickel–Alkyl Complexes with a Reactive PNC-Pincer Ligand

Linda S. Jongbloed,[a] Nicolas Vogt,[b] Aaron Sandleben,[b] Bas de Bruin,[a] Axel Klein*[b] and Jarl Ivar van der Vlugt*[a]

Abstract: Based on previous work related to the design and application of rigid tridentate phosphine–pyridine–phenyl coordination offered by a PNC-pincer ligand upon cyclometalation to nickel, the synthesis, spectroscopic and solid state characterization and redox-reactivity of two Ni^{II}(PNC) complexes featuring either a methyl (**2CH$_3$**) or CF_3 co-ligand (**2CF$_3$**) are described. One-electron oxidation is proposed to furnish C–C reductive elimination, as deduced from a combined chemical, electrochemical, spectroscopic and computational study. One-electron reduction results in a ligand-centered radical anion, as supported by electrochemistry, UV spectroelectrochemistry, EPR spectroscopy, and DFT calculations. This further attenuates the breadth of chemical reactivity offered by such PNC-pincer ligands.

Introduction

Nickel–alkyl species have become relevant for a wide variety of C–C bond-forming reactions, including Negishi, Suzuki–Miyaura, Stille, Kumada and Hiyama couplings.[1,2] The trifluoromethylation of arenes is industrially interesting because of the intriguing properties of fluoroorganic materials.[3] In late transition metal complexes, the CF_3 substituent is usually strongly bound to the metal center and is therefore often not susceptible to reductive elimination.[4] It was proposed that Ni could be an active catalyst for this transformation,[5,6] and the precise understanding of Ni–CF_3 bonding and reactivity of these complexes have been subject to several studies, usually in comparison to Ni–CH_3 bonding.[7–12] The main findings show that the lone pair of the carbanionic CF_3 ligand has increased C 2s character and a stronger donation to the metal compared to the methyl analog. Furthermore, complexes with a CF_3 ligand usually show higher oxidation potentials compared to the corresponding CH_3 complexes.

Most previously reported mechanistic investigations and model systems for C–C coupling at Ni focus on cross-coupling reactions, in which the target phenyl ligand can freely rotate around the M–Ph bond.[13] A recent model system that has proven very useful in this context is based on *N*,*N*′-di-*tert*-butyl-2,11-diaza[3,3](2,6)pyridinophane as ligand (Scheme 1A).[14] We herein report complexes with a cyclometalated Ni^{II} center, in which the rotation of the phenyl ligand is constrained by the linkage to the adjacent pyridine moiety (Scheme 1B). These species can be regarded as model systems for the recently reported Ni-catalyzed C–H functionalization reactions of substrates with a bidentate 8-aminoquinoline directing group (Scheme 1C).[15,16] Besides one theoretical investigation of the mechanism of this type of reaction,[17] little information is available on the elementary steps for substrate activation and product formation. Inspired by this observation and given our interest in bifunctional substrate activation using reactive ligands[18] as well as applications of redox-active ligands,[19] we set out to study the chemistry of model Ni–alkyl complexes bearing a pincer ligand featuring a flanking aryl fragment.

We previously reported a new family of **P^{X}NC** pincer ligands **L^{X}H** (X = CH_2 or O; Scheme 2) that are susceptible to facile reversible cyclometalation at the flanking phenyl substituent in the case of Rh^I precursor complexes.[20] We also reported selective reprotonation of the Rh–C_{Ph} bond to afford the crystallographically characterized complex [RhCl(CO)(κ^2-*P*,*N*-**HL^{CH2}**)] with a reprotonated phenyl substituent that is still in the first coordination sphere of Rh^I. This platform also enabled Rh-catalyzed formic acid dehydrogenation using the metal–ligand bifunctional strategy.[21] Satisfyingly, the same flexible coordination chemistry was available with nickel, including base-mediated cyclometalation directly from a Ni^{II} precursor to provide a [Ni^{II}Br(κ^3-*P*,*N*,*C*-**P^{O}NC**)] complex and subsequent reprotonation of the nickel–C_{Ph} bond.[22]

Beyond the reversible nature of the nickel–carbon bond, the cyclometalated nickel species also offers substitution chemistry at the Ni–Br fragment. We therefore decided to synthesize square planar [Ni^{II}(alkyl)(κ^3-*P*,*N*,*C*-**P^{O}NC**)] complexes that contain either a CH_3 or CF_3 as alkyl ligand. Oxidation of such a Ni–CF_3 complex is expected to occur at more positive potential than

[a] *Homogeneous, Bioinspired and Supramolecular Catalysis, van 't Hoff Institute for Molecular Sciences, University of Amsterdam, Science Park 904, 1098 XH Amsterdam, The Netherlands*
E-mail: J.I.vanderVlugt@uva.nl
http://www.homkat.nl
[b] *Department für Chemie, Institut für Anorganische Chemie, Universität zu Köln, Greinstraße 6, 50939 Köln, Germany*
E-mail: axel.klein@uni-koeln.de
http://www.klein.uni-koeln.de/

Supporting information and ORCID(s) from the author(s) for this article are available on the WWW under https://doi.org/10.1002/ejic.201800168.

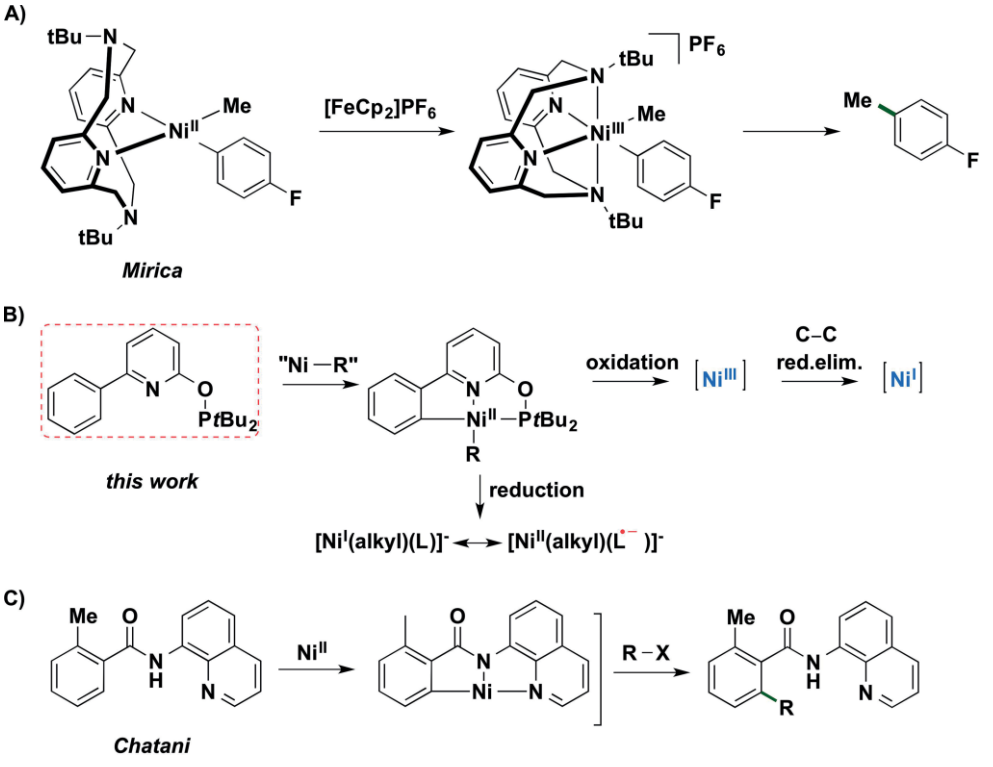

Scheme 1. (A) a recently published model for aryl–alkyl coupling (adapted from ref.[14]). (B) the model system for a constrained phenyl ligand used in this work. (C) C–H functionalization using the directing group approach (adapted from ref.[15]).

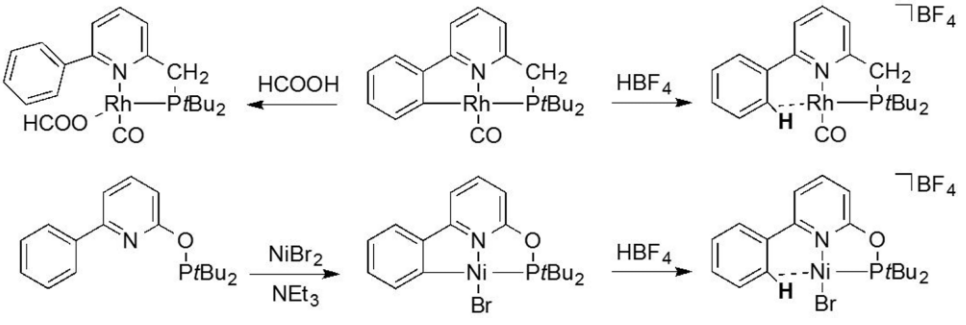

Scheme 2. Reversible cyclometalation reactivity of novel $\mathbf{P^XNC}$-pincer platforms $\mathbf{L^XH}$ with Rh^I and Ni^{II}.

for the corresponding Ni–CH_3 complex and the resulting Ni^{III} species, relevant in the context of C_{Ar}–C_{alkyl} reductive elimination, may potentially be detectable.[23] Previous reports show that CF_3 ligands can stabilize the Ni^{III} oxidation state in $[Ni^{III}(tBu_3tpy)(CF_3)_2]^{\bullet+}$ (tBu_3tpy = 4,4′,4″-tris(*tert*-butyl)-2,2′:6,2″-terpyridine).[24] Reductive elimination from Ni^{III} would result in formation of a formally Ni^I species, which are also considered of relevance, e.g., for cross-coupling catalysis and for metalloradical-induced reactivity.[25]

One-electron reduction of the Ni^{II}–alkyl complexes might lead to the formation of Ni^I species $[Ni^I(alkyl)(\kappa^3\text{-}P,N,C\text{-}\mathbf{P^ONC})]^-$ or alternatively to Ni^{II} complexes with a radical anionic ligand $[Ni^{II}(alkyl)(\kappa^3\text{-}P,N,C\text{-}\mathbf{P^ONC}^{\bullet-})]^-$ and the nature of the alkyl ligand might be decisive for the specific character of these reduced species. This is in analogy to tpy complexes with $[Ni(tpy)(R)]^\bullet$ (R = alkyl or aryl) that show clear evidence for Ni^{II} coordinated to reduced $tpy^{\bullet-}$, while $[Ni(tpy)(X)]^\bullet$ (X = I, Br, Cl) species are best described as Ni^I species.[26]

We used a combination of cyclic voltammetry, UV/Vis spectroelectrochemistry, and chemical oxidants or reductants in combination with EPR spectroscopy and supported by DFT calculations to study the redox chemistry of these two complexes in detail on which we will report herein. These findings may be relevant not only for the modelling of carbon–carbon bond forming reactions but also in the application of redox-active ligands in catalysis, which is an emerging field of research.

Results and Discussion

Complexes $\mathbf{2CH_3}$ and $\mathbf{2CF_3}$ are both synthesized from the previously reported complex **1**.[22] The Me group in complex $\mathbf{2CH_3}$

can be easily installed via simple transmetalation using MeLi and **1** in toluene (Scheme 3), which results in an immediate color change from yellow to red. The desired product shows a small downfield shift in ^{31}P NMR compared to complex **1** (δ = 194 ppm vs. 187 ppm) and the corresponding ^{1}H NMR spectrum contains an upfield signal at δ = –0.06 ppm ($^{3}J_{PH}$ = 9.1 Hz) that is assigned to the Ni-bound CH_3 ligand. Crystals suitable for X-ray analysis were grown by slow evaporation of an Et_2O solution (Figure 1) and the molecular structure shows Ni–CH_3 bond lengths of 1.933(4) Å, 1.943(4) Å, 1.957(4) Å and 1.958(4) Å for the four independent molecules found in the asymmetric unit cell (more details in the Experimental Section). Complex **2CF$_3$** is prepared by reacting **1** with CsF and TMS–CF_3, Ruppert's reagent,[27] in THF. Complex **2CF$_3$** shows a quartet in ^{31}P NMR at δ = 195 ppm with a coupling constant $^{3}J_{PF}$ of 26 Hz and a doublet at δ = 11 ppm with the same coupling constant is found in ^{19}F NMR spectroscopy. In the ^{13}C NMR spectrum a signal is evident for the CF_3 ligand at δ = 144 ppm with a coupling constant $^{2}J_{PC}$ of 18 Hz and a large coupling constant $^{1}J_{CF}$ of 357 Hz, which is similar to other reported Ni–CF_3 complexes.[8,28] Single crystals of **2CF$_3$** were obtained by slow solvent evaporation from a solution of **2CF$_3$** in diethyl ether. The molecular structure is similar to complex **2CH$_3$** although the Ni–CF_3 bond is slightly contracted in comparison to the Ni–CH_3 bond [1.878(3) Å; Δd vs. Ni–CH_3 of at least 0.055 Å]. This phenomenon is common and can be explained by the stronger binding of the CF_3 group to Ni. Another reported difference between Ni–CH_3 and Ni–CF_3 complexes is the stabilization of the HOMO and the LUMO by the CF_3 ligand.[4,11,12]

To analyze whether this also holds for complexes **2CH$_3$** and **2CF$_3$**, we resorted to DFT calculations. After structure optimization, the energy levels of the frontier molecular orbitals were determined. Table 1 shows the comparison of the energy levels of the HOMO and LUMO of **2CH$_3$** and **2CF$_3$**. The calculated HOMO of complex **2CF$_3$** is stabilized by 0.5 eV relative to **2CH$_3$**, which will probably result in a higher oxidation potential for **2CF$_3$**. On the other hand, also the LUMO of **2CF$_3$** is stabilized by 0.3 eV, which should translate to reduction at less negative potential.

Table 1. DFT[a] calculated energy levels of the frontier orbitals of complexes **2CH$_3$** and **2CF$_3$**.

	HOMO [eV]	LUMO [eV]	Gap [eV]
Complex **2CH$_3$**	–4.215	–2.432	1.783
Complex **2CF$_3$**	–4.679	–2.747	1.932

[a] Structures optimized with Turbomole (BP86, def2-TZVP, disp3).

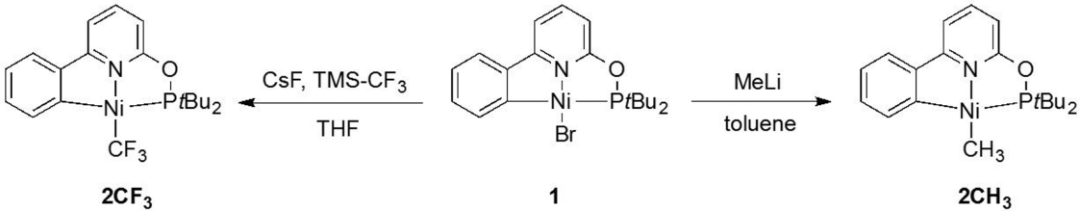

Scheme 3. Synthesis of Ni–alkyl complexes **2CH$_3$** and **2CF$_3$** from precursor **1**.

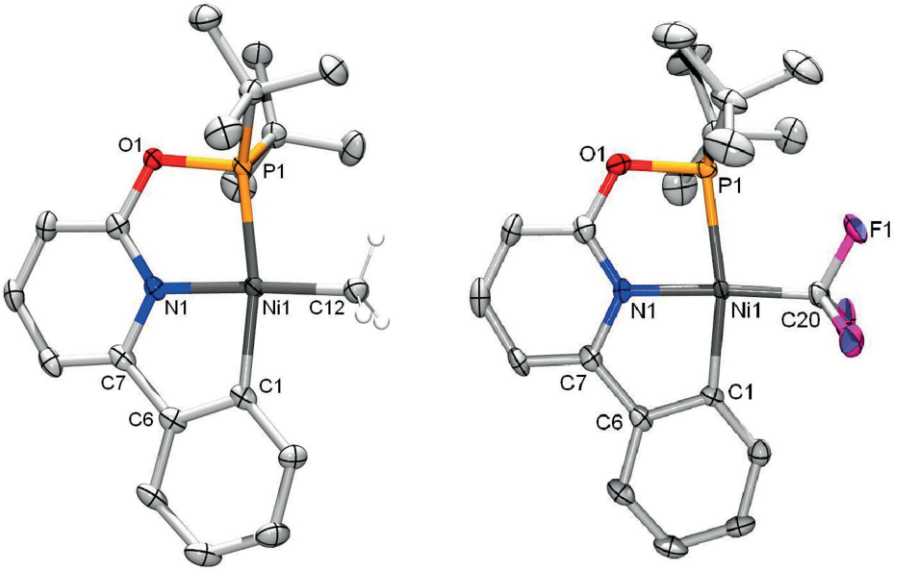

Figure 1. ORTEP plots (50 % probability) for **2CH$_3$** (left) and **2CF$_3$** (right) (See Experimental Section for details). Selected bond lengths [Å] and angles [°] for **2CH$_3$**: Ni1–C12 1.933(4); Ni1–C1 1.925(3); Ni1–N1 1.902(3); Ni1–P1 2.151(1); C1–Ni1–N1 84.0(1); C1–Ni1–C12 93.4(2); C12–Ni1–P1 99.7(1); P1–Ni1–N1 83.0(1); C1–Ni1–P1 166.7(1). For **2CF$_3$**: Ni1–C20 1.878(3); Ni1–C1 1.944(3); Ni1–N1 1.906(2); Ni1–P1 2.213(1); N1–Ni1–C1 84.3(1); C20–Ni1–C1 92.8(1); P1–Ni1–N1 82.69(9); P1–Ni1–C20 100.4(1); C1–Ni1–P1 166.1(1).

The stabilizing effect of the CF_3 ligand was also apparent by mass spectrometry. For complex **2CF$_3$** the molecular ion peak was observed using Electron Spray Ionization (ESI) at *m/z* 442.1077, while only fragmented ion peaks were found for complex **2CH$_3$**. Field Desorption (FD), showed a main fragmentation at *m/z* 345.2762 for **2CH$_3$**, which could correspond to a methylated ligand structure with a phosphine oxide (calculated mass of 345.1858). This result indicates that complex **2CH$_3$**, in contrast to complex **2CF$_3$**, is relatively unstable toward reductive elimination upon ionization.

Oxidation of Ni^{II} Species 2CH$_3$ and 2CF$_3$

The electrochemistry of both alkyl complexes was probed with cyclic voltammetry. For complex **2CH$_3$**, the cyclic voltammogram in PrCN revealed irreversible oxidation events at –0.08 V and +0.77 V, regardless of the temperature (room temp. or –55 °C) or scan rate (Figure 2, left). For **2CF$_3$** a first irreversible oxidation wave was observed at +0.51 V, with an equally irreversible follow-up event at +0.88 V. Thus, the alkyl ligand has a strong impact on the oxidation processes, in line with a metal-centered (Ni^{II}/Ni^{III}) oxidation. These redox events, postulated to forming Ni^{III} intermediate species, are likely coupled to follow-up C–C bond-forming reductive elimination of the alkyl fragment and the phenyl ring of the PNC ligand, generating a Ni^{I} complex **A** with the ligand only coordinating via the P and the N donors, as well as solvent molecules to fulfil the coordination sphere requirements around Ni. Chemical oxidation of **2CH$_3$** at room temp. in a mixture of PrCN/MeCN (3:1) using the mild oxidant [acetylferrocenium]BF_4 ([Fe(η^5-$C_5H_4C(O)Me$)(η^5-C_5H_5)]-BF_4) led to a color change from dark blue to orange. EPR spectroscopy of the frozen sample at 30 K revealed a well-defined rhombic spectrum (Figure 2, middle) with well-resolved hyperfine interactions related to a single phosphorus atom. This spectrum could be simulated with the *g*- and *A*-tensor components shown in Table 2. Reductive elimination of the one-electron oxidized species [Ni^{III}(Me)(κ^3-*P,N,C*-**P^{O}NC**)]$^+$ would lead to a C_{alkyl}–C_{Ph} bond in a [Ni^{I}(κ^2-*P,N*-**P^{O}NC**-Me)]$^+$ species with a pending tolyl group at the phosphino–pyridine ligand. DFT calculations of the EPR parameters for the optimized geometry of solvated Ni^{I} complex **A**, [Ni^{I}(NCMe)$_2$(κ^2-*P,N*-**P^{O}NC**-Me)]$^+$ [structure optimized with Turbomole (BP86, def2-TZVP, disp3)] showed good agreement with the experimentally obtained EPR data, using either ORCA or ADF (Figure 2, right). The calculated EPR parameters of the putative optimized Ni^{III} species **B**, [Ni(CH_3)(NCMe)(κ^3-*P,N,C*-**P^{O}NC**)]$^+$ were very different, with a nearly axial *g* tensor and much smaller phosphorus hyperfine interactions (Table 2).

Table 2. Experimental and DFT calculated EPR parameters of **A**, [Ni^{I}(NCMe)$_2$(κ^2-*P,N*-**P^{O}NC**-Me)]$^+$ and the putative Ni^{III} intermediate.

	Experimental[a]	DFT			
		(ORCA)[b] Ni^{I} **A**	(ADF)[c] Ni^{I} **A**	(ORCA)[b] Ni^{III} **B**	(ADF)[c] Ni^{III} **B**
g_x	2.277	2.185	2.197	2.206	2.219
g_y	2.150	2.114	2.127	2.195	2.204
g_z	2.025	2.027	2.025	2.021	2.018
A_x^P	214	196	210	–19	–19
A_y^P	230	264	270	–13	–13
A_z^P	235	207	221	–12	–12
$\rho^{P[d]}$		0.12		–0.02	
$\rho^{Ni[d]}$		0.74		0.83	

[a] Values obtained by spectral simulation. [b] ORCA, B3LYP, def2-TZVP. [c] ADF, B3LYP, TZ2P, SOC, ZORA, unrestricted, collinear. [d] Atomic spin populations (Turbomole, BP86, def2-TZVP, disp3).

These results are in line with anodic UV/Vis spectroelectrochemistry of complex **2CH$_3$** (Figure 3), which clearly shows the bleaching of the long-wavelength band at 454 nm, presumably corresponding to a metal-to-ligand charge transfer (MLCT) and the blue shift of a π–π^* band at 315 nm to 292 nm indicating both the reduction of the metal. Furthermore, **2CH$_3$** and **2CF$_3$** were anodically oxidized in the presence of the spin trap PBN (*N-tert*-butyl-α-phenylnitrone) in the EPR cavity but no signals of PBN adducts of either alkyl fragment, indicative for the formation of $\cdot CH_3$ or $\cdot CF_3$ radicals, were observed. Such signals have been observed upon oxidation of the complexes [Ni(BOXAM)(alkyl)] (BOXAM = bis((4-isopropyl-4,5-dihydrooxaz-

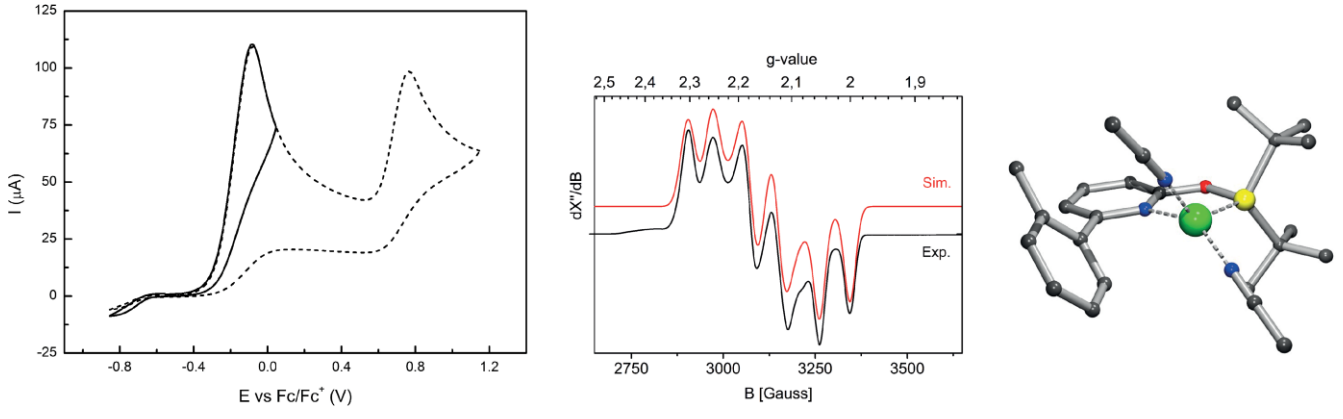

Figure 2. Left: cyclic voltammograms of a 6 mM solution of **2CH$_3$** in PrCN/N(nBu)$_4$PF$_6$ at 298 K, with a scan rate of 100 mV/s. Middle: Experimental and simulated X-band EPR spectra of proposedly complex **A**, [Ni^{I}(NCMe)$_2$(κ^2-*P,N*-**P^{O}NC**-Me)]$^+$. The simulated spectrum was obtained using the parameters listed in Table 2. The experimental spectrum was recorded at 30 K in frozen PrCN/MeCN 3:1. Microwave frequency = 9.363973 GHz, modulation amplitude = 4 Gauss, microwave power = 2 mW. Right: Optimized geometry (Turbomole BP86, def2-TZVP, disp3) of the suggested geometry of the Ni^{I} complex [Ni^{I}(NCMe)$_2$(κ^2-*P,N*-**P^{O}NC**-Me)]$^+$.

ol-2-yl)phenyl)amine) bearing either CH_3 or CF_3 as alkyl ligand, which suggest formation of a species containing Ni^{II} and the oxidized BOXAM ligand (aminyl radical).[9]

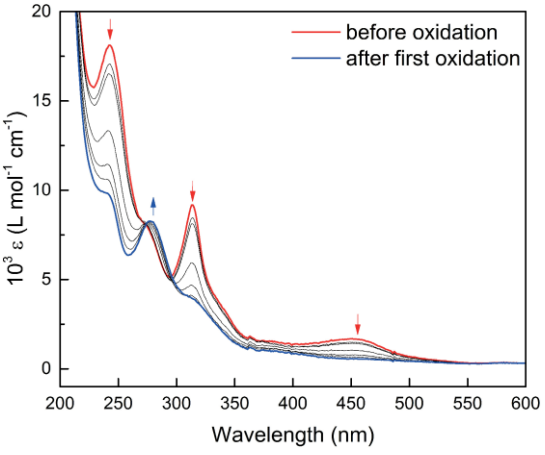

Figure 3. UV/Vis spectroelectrochemical oxidation of a solution of complex **2CH$_3$** in THF/N(*n*Bu)$_4$PF$_6$; anodic scan from 0 V to +1.2 V (referenced to Ag/Ag$^+$).

Use of one equiv. $AgBF_4$ as chemical oxidant in MeCN led to a precipitate and still ±50 % starting complex **2CH$_3$**, judging from UV/Vis spectroscopy, whereas with two equiv. $AgBF_4$ a well-defined new signal at δ = 2.26 ppm in the ^{1}H NMR spectrum was detected, assigned to the Ph–CH_3 group (Figure 4, left). Furthermore, the aromatic region showed typical signals for a freely rotating phenyl ring, rather than a cyclometalated analog, that integrate for four protons. The ^{31}P NMR spectrum showed two slightly broadened overlapping doublets (Figure 4, right) at δ = 139.1 ppm, $^1J_{Ag\text{-}P}$ = 707 Hz (^{107}Ag isotope) and $^1J_{Ag\text{-}P}$ = 618 Hz (^{109}Ag isotope), plus an even more broadened side product with similar features. These combined spectroscopic data correspond well with those of related complexes already reported by Klausmeyer.[29] The main product is thus attributed to a dimeric Ag complex with the phosphino–pyridine ligand acting as a bridging dinucleating framework in [Ag_2(κ^2-*P*,*N*-**P^{O}NC**-Me)$_2$] (**B**). This species would be formed upon transfer of the ligand from Ni^I to Ag^I. The observed NMR broadening likely corresponds to fast reversible dissociation of the phosphine donors.[29] Using high resolution cold-spray ionization (CSI) mass spectrometry a molecular ion peak was detected at *m*/*z* = 477.1248, supporting the formation of this dinuclear silver species **B**.

Transmetalation of the ligand from Ni^I to Ag^I upon C–C reductive elimination was also supported by the rudimentary detection of crystalline [Ni^{II}(NCMe)$_6$](BF$_4$)$_2$ (by X-ray diffraction) that separated from the reaction mixture, which may suggest a disproportionation reaction of unstable [Ni^I(NCMe)$_x$]BF_4 into a Ni^0 species and the aforementioned characterized Ni^{II} species. The oxidation of **2CF$_3$** with (thianthrenium)BF_4 in [D_3]MeCN in the presence of $AgBF_4$ led to similar ^{31}P NMR features, whilst the ^{19}F NMR spectrum contained a signal at δ = –57 ppm, indicative of the formation of a C_{Ph}–C_{CF3} fragment via reductive elimination.[30] CSI-HRMS also supported formation of the dinuclear Ag complex after transmetalation, with a molecular ion peak at *m*/*z* 531.0953. (Scheme 4).

Reduction of Ni^{II} Species 2CH$_3$ and 2CF$_3$

To probe any possible reduction events with both alkyl species, we again initially resorted to cyclic voltammetry. The cyclic voltammograms of **2CH$_3$** and **2CF$_3$** show a reversible reduction wave at $E_{1/2}$ = –2.60 V and –2.36 V, respectively (Figure 5). The

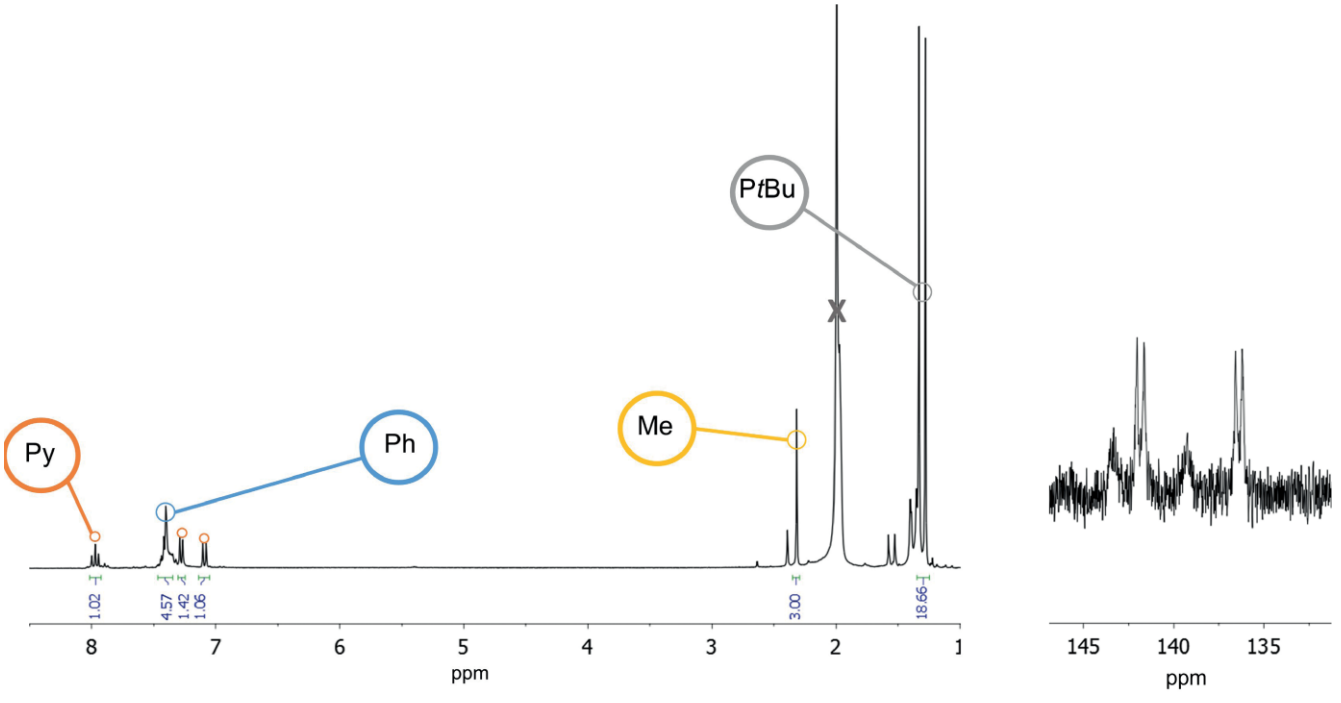

Figure 4. Left: ^{1}H NMR spectrum in [D_3]MeCN from the reaction of complex **2CH$_3$** with two equivalents of $AgBF_4$. Right: corresponding ^{31}P NMR spectrum.

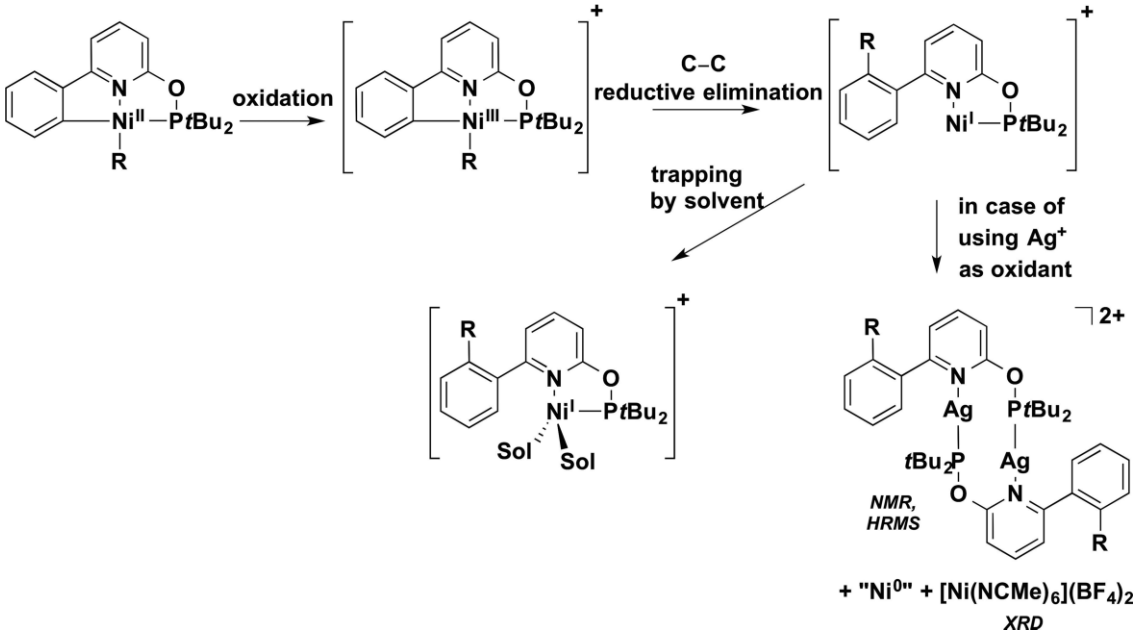

Scheme 4. Postulated sequence of reactions upon one-electron oxidation of **2CH$_3$** or **2CF$_3$**.

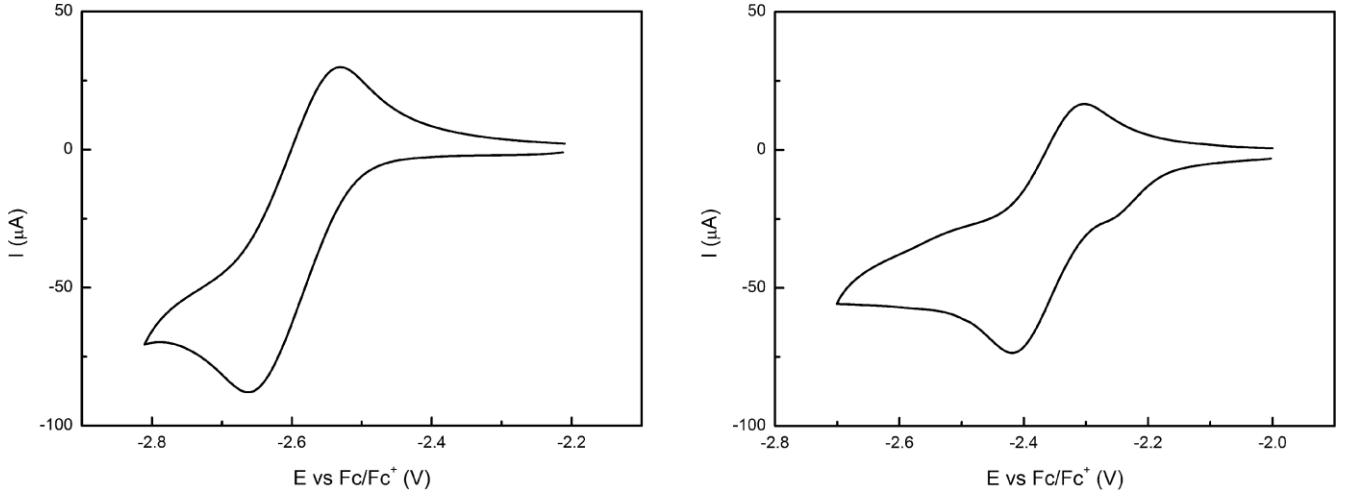

Figure 5. Cyclic voltammograms, reductive scans, of a 6 mM solution of **2CH$_3$** (left) and **2CF$_3$** (right) in PrCN/N(*n*Bu)$_4$PF$_6$ at 298 K, at a scan rate of 100 mV/s.

observed difference in reduction potentials of **2CH$_3$** and **2CF$_3$** is in agreement with the DFT calculations, which predicted that the reduction of **2CF$_3$** would occur at a higher potential due to stabilization of the LUMO by the CF_3 ligand. Both processes seem to be reversible at the scan speed of 100 mV/s, although the wave of **2CF$_3$** has a small shoulder which is most likely a small impurity.

UV/Vis spectroelectrochemistry was performed in THF, in which both complexes show similar behavior. The reduction event of **2CH$_3$** occurs at very negative potential, resulting in interference of solvent reduction. This problem is not observed for **2CF$_3$** and upon spectroelectrochemical reduction, three new broad and partially structured band systems in the NIR and visible region appear with maxima at λ = 1090, 661 and 430 nm, and one intense new band in the UV region at λ 324 nm, while the initial bands at 393 and 343 nm either shift to higher energy or disappear (Figure 6). The very intense band at λ 245 nm is reduced in intensity to about 50 %. These features are reminiscent of the ligand-centered reduction of bipyridine complexes, e.g. quite similar absorptions were recently reported for the radical anionic Ni^{II} complex [Ni^{II}Br(Phbpy)$^{\bullet-}$]$^-$ (HPhbpy = 6-phenyl-2,2′-bipyridine).[31] The combined data clearly indicate a reduction centered at the phenylpyridine core of the ligand of **2CF$_3$** to furnish complex **[3CF$_3$]$^{\bullet-}$**, which is best described as Ni^{II} bound to a radical anionic ligand [Ni^{II}(CF$_3$)(κ^3-*P*,*N*-**P^{O}NC**)$^{\bullet-}$]$^-$ rather than a Ni^I complex. To find further evidence to support that the reduction is ligand centered, complexes **2CH$_3$** and **2CF$_3$** were treated with KC_8 in THF, resulting in a slight darkening of the solutions (Scheme 5).

The EPR spectrum of compound **[3CH$_3$]$^{\bullet-}$** measured in isotropic solution is characteristic for a ligand–radical complex and reveals a set of well-resolved hyperfine couplings (Figure 7). A

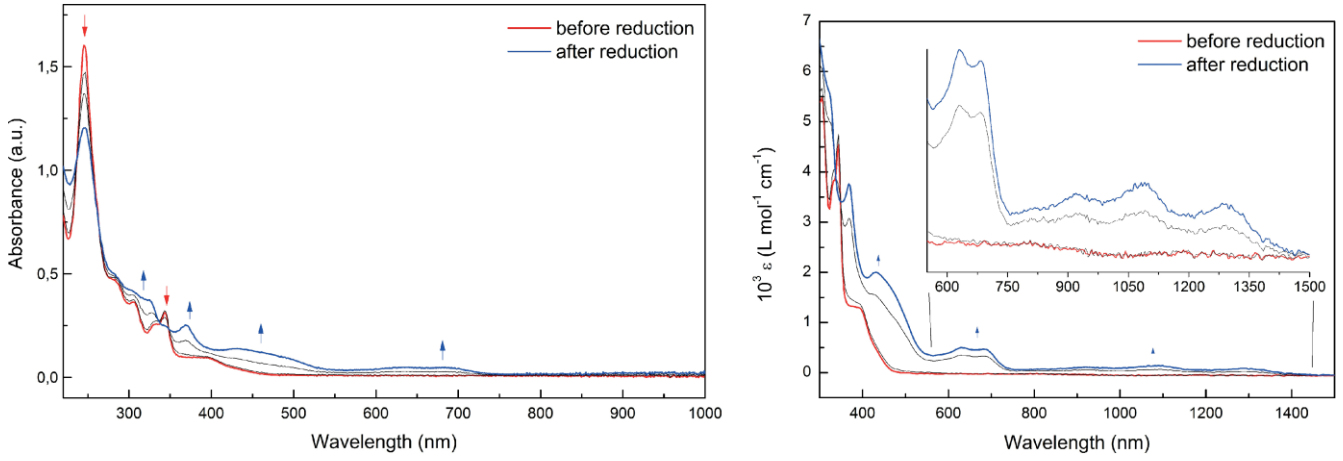

Figure 6. UV/Vis spectroelectrochemical reduction of complex **2CF$_3$** in THF/N(*n*Bu)$_4$PF$_6$; cathodic scan from 0 V to −2.2 V (referenced to Ag/Ag$^+$).

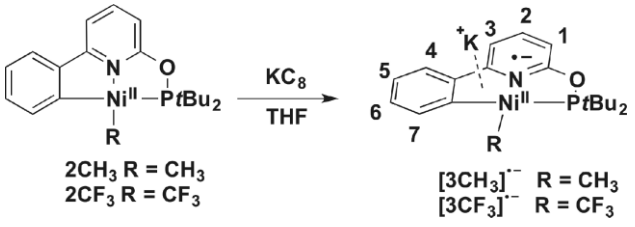

Scheme 5. Proposed anionic ligand radical species **[3CH$_3$]**$^{\bullet-}$ and **[3CF$_3$]**$^{\bullet-}$ from reaction of **2CH$_3$** and **2CF$_3$** with KC_8.

Table 3. Experimental and DFT calculated EPR parameters of **[3CH$_3$]**$^{\bullet-}$.

	Exp.[a]	DFT (ORCA)[b]	DFT (ADF)[c]
g_{iso}	2.007	2.003	2.003
A^P_{iso}	−10.5	−13.1	−14.0
A^N_{iso}	5.0	5.9	6.6
A^{H1}_{iso}	−7.0	−9.6	−10.4
A^{H2}_{iso}	−8.5	−14.3	−15.9
A^{H3}_{iso}	NR	3.0	3.5
A^{H4}_{iso}	−6.5	−6.9	−7.8
A^{H5}_{iso}	NR	2.4	3.0
A^{H6}_{iso}	−8.0	−10.7	−11.6
A^{H7}_{iso}	NR	3.3	3.8

[a] Values obtained by spectral simulation. [b] ORCA, B3LYP, def2-TZVP. [c] ADF, B3LYP, TZ2P.

satisfactory simulation was obtained with the parameters shown in Table 3 and DFT computed EPR parameters are in agreement with the experimental data. A very similar EPR spectrum (see Supporting Information) was obtained through cathodic reduction of **2CH$_3$** in N(*n*Bu)$_4$PF$_6$/THF in the EPR cavity (EPR spectroelectrochemistry).

For complex **[3CF$_3$]**$^{\bullet-}$ a similar signal was observed in EPR, although the hyperfine splitting was less resolved (see Supporting Information). The combined data strongly indicate the formation of a PNC ligand radical anion formed in the coordination sphere of Ni^{II}, with the unpaired electron spread out across most of the phenyl–pyridine framework, as deduced from the DFT computed electronic structure of **[3CH$_3$]**$^{\bullet-}$ – the SOMO and spin density plots of **[3CH$_3$]**$^{\bullet-}$ are shown in Figure 6 (middle and right, respectively).

Thus, both reduced complexes **[3CH$_3$]**$^{\bullet-}$ and **[3CF$_3$]**$^{\bullet-}$ are best described as Ni^{II} complexes containing a radical anionic **P^{O}NC** ligand [Ni^{II}(alkyl)(κ^3-*P,N,C*-**P^{O}NC**$^{\bullet-}$)]$^-$ in analogy to the previously

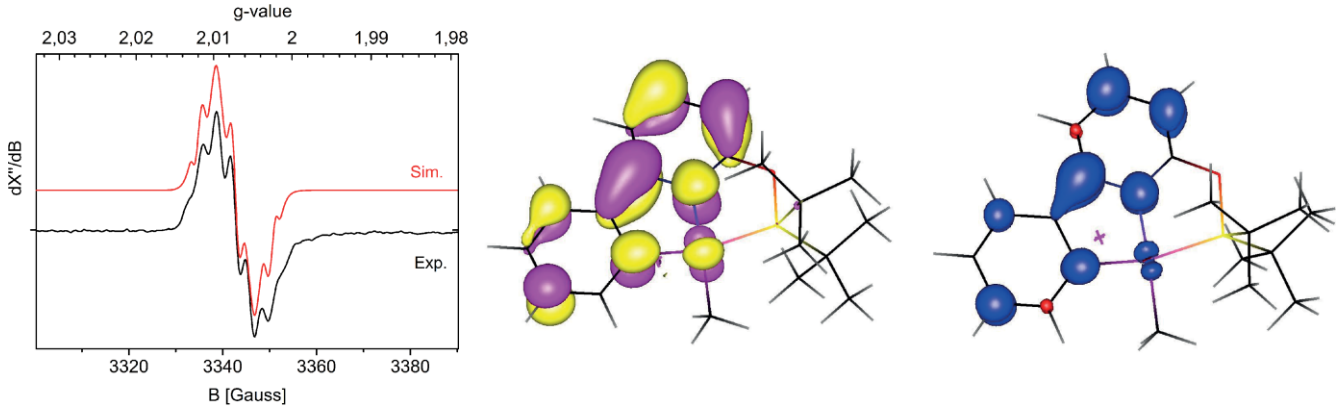

Figure 7. Left: Experimental and simulated X-band EPR spectra of Ni^{II}–ligand radical complex **[3CH$_3$]**$^{\bullet-}$ measured in isotropic solution (THF) at room temp. Experimental conditions: Temperature = 298 K, microwave power 2.0 mW, field amplitude = 1 Gauss, microwave frequency = 9.390764 GHz. The simulated spectrum was obtained with the parameters shown in Table 3. (Middle) SOMO of complex **[3CH$_3$]**$^{\bullet-}$ (Turbomole, BP86, def2-TZVP). (Right) Spin density plot of complex **[3CH$_3$]**$^{\bullet-}$ (Turbomole, BP86, def2-TZVP).

studied radical complex species [Ni^{II}(R)(terpy$^{\bullet-}$)] (terpy = 2,2′:6,2″-terpyridine) with R = alkyl or aryl.[26] In the context of our current interest to bridge the fields of redox-active and reactive ligand design, these findings of ligand-centered one-electron reduction of the cyclometalated PNC platform, which was already shown to be chemically responsive in our previous work,[20–22] may prove a step in this direction.

Conclusions

The four-coordinate nickel–alkyl complexes [Ni^{II}(alkyl)(κ^3-*P,N,C*-**P^{O}NC**)] with alkyl = CH_3 (**2CH$_3$**) or CF_3 (**2CF$_3$**), stabilized by a cyclometalated PNC pincer ligand have been synthesized and fully characterized. Both complexes show irreversible oxidation events in cyclic voltammetry that are likely coupled to C–C bond-forming reductive elimination. Bulk oxidation experiments yielded strong evidence for a Ni^{I} complex from EPR spectroscopy and DFT calculations on the assumed species [Ni^{I}(κ^2-*P,N*-**P^{O}NC**-Me)(MeCN)$_2$]$^+$ containing a pendant 2-tolyl group from reductive C_{alkyl}–C_{Ph} bond formation, gave EPR parameters fully in line with the experimental data. Moreover, these complexes show reversible reduction, as judged from a combined experimental and computational study including spectroelectrochemistry, EPR spectroscopy and DFT calculations. Both spectroelectrochemistry and EPR point out that it is possible to reduce the phenylpyridine core of the ligand to produce a ligand-centered radical. In this way, the cyclometalated PNC platform which was already shown to be chemically responsive, can be included into the family of non-innocent ligands.[32]

Experimental Section

General Methods: All reactions were carried out under an atmosphere of nitrogen using standard Schlenk techniques. Reagents were purchased from commercial suppliers and used without further purification. THF, *n*-pentane, *n*-hexane and Et_2O were distilled from sodium benzophenone ketyl, CH_2Cl_2 was distilled from CaH_2, toluene from sodium under nitrogen. NMR spectra (^{1}H, ^{31}P, and ^{13}C(^{1}H)) were measured on a Bruker DRX 500, Bruker AV 400, Bruker DRX 300 or on a Bruker AV 300 spectrometer. A Shimadzu UV 2700 spectrophotometer was used to record UV/Vis spectra. High resolution mass spectra were recorded on a JMS-T100GCV mass spectrometer using field desorption (FD), or JEOL AccuTOF LC, JMS-T100LP mass spectrometer using electron-spray ionization (ESI or CSI). Complex **1**, [NiBr(κ^3-*P,N,C*-**P^{O}NC**)] was synthesized as previously reported by us.[22]

[Ni(CH$_3$)(κ^3-*P,N,C*-P^{O}NC)] (complex 2CH$_3$): Complex **1** (0.080 g, 0.18 mmol) was dissolved in toluene (5 mL) and MeLi (1.6 M in Et_2O) (110 μL, 0.18 mmol) was added, resulting in a color change from orange to red. After stirring for 5 min, the suspension was filtered through Celite and the solvent evaporated. The product was extracted with *n*-pentane (15 mL), filtered and dried in vacuo to yield **2CH$_3$** as a bright orange solid (0.055 g, 80 %). Crystals suitable for X-ray analysis were grown by slow evaporation of an Et_2O solution. ^{1}H NMR (300 MHz, [D$_3$]MeCN, ppm): δ = 7.77 (vt, J = 7.9 Hz, 1 H, Py-CH), 7.51 (dt, J = 7.5, 1.7 Hz, 1 H, Ph-CH), 7.46–7.37 (m, 1 H, Ph-CH), 7.32 (dd, J = 7.7, 0.8 Hz, 1 H, Py-CH), 7.20 (tt, J = 7.3, 1.7 Hz, 1 H, Ph-CH), 7.04 (td, J = 7.4, 1.4 Hz, 1 H, Ph-CH), 6.80 (d, J = 8.2 Hz, 1 H, Py-CH), 1.41 [d, $^3J_{PH}$ = 13.6 Hz, 18 H, $(CH_3)_3$CP], –0.06 (d, $^3J_{PH}$ = 9.1 Hz, 3 H, Ni-CH_3). ^{31}P NMR (121 MHz, [D$_3$]MeCN, ppm): δ = 194.28. ^{13}C NMR (75 MHz, [D$_3$]MeCN, ppm): δ = 165.74 (d, $^2J_{PC}$ = 92.2 Hz, Ni-C), 164.73 (d, J_{PC} = 4.5 Hz, Py-C), 164.01 (d, J_{PC} = 9.5 Hz, Py-C), 150.28 (s, Ph-C), 141.79 (s, Py-CH), 134.37 (s, Ph-CH), 130.21 (d, J_{PC} = 5.3 Hz, Ph-CH), 125.09 (s, Ph-CH), 123.09 (d, J_{PC} = 3.5 Hz, Ph-CH), 111.62 (s, Py-CH), 107.11 (d, J_{PC} = 4.0 Hz, Py-CH), 39.16 [d, $^1J_{PC}$ = 4.2 Hz, $(CH_3)_3$CP], 27.82 [d, $^2J_{PC}$ = 6.8 Hz, $(CH_3)_3$CP], –10.92 (d, $^2J_{PC}$ = 14.7 Hz, Ni-CH_3). UV/Vis (MeCN, nm): λ = 241 (ε = 1.7 × 10^4 L mol^{-1} cm^{-1}), 313 (ε = 7.8 × 10^3 L mol^{-1} cm^{-1}), 452 (ε = 1.3 × 10^3 L mol^{-1} cm^{-1}).

[Ni(CF$_3$)(κ^3-*P,N,C*-P^{O}NC)] (2CF$_3$): THF (10 mL) was added to a Schlenk containing complex **1** (0.080 g, 0.18 mmol) and CsF (0.080 g, 0.53 mmol). After stirring for 20 min, TMS-CF_3 (2.0 M in THF) (0.27 mL, 0.53 mmol) was added dropwise and the reaction was stirred overnight. Subsequently, more TMS-CF_3 (0.13 mL, 0.27 mmol) was added and the reaction was stirred for an additional four hours. THF was evaporated and the product was extracted with *n*-pentane. After filtration, the solvent was evaporated to yield **2CF$_3$** as a yellow solid (0.078 g, quantitative). Crystals suitable for X-ray analysis were grown by slow evaporation of an Et_2O solution. ^{1}H NMR (300 MHz, [D$_3$]MeCN, ppm): δ = 7.84 (vt, J = 8.0 Hz, 1 H, Py-CH), 7.56–7.43 (m, 2 H, Ph-CH), 7.34 (d, J = 7.7 Hz, 1 H, Py-CH), 7.20–7.04 (m, 2 H, Ph-CH), 6.82 (d, J = 8.2 Hz, 1 H, Py-CH), 1.45 [d, $^3J_{PH}$ J = 14.2 Hz, 18 H, $(CH_3)_3$CP]. ^{31}P NMR (121 MHz, [D$_3$]MeCN, ppm): δ = 194.96 (q, $^3J_{PF}$ = 25.8 Hz). ^{19}F NMR (282 MHz, [D$_3$]MeCN, ppm): δ = –10.93 (d, $^3J_{PF}$ = 25.6 Hz). ^{13}C NMR (126 MHz, [D$_3$]MeCN, ppm): δ = 165.69 (d, J_{PC} = 3.6 Hz, Py-C), 164.34 (d, J_{PC} = 9.3 Hz, Py-C), 161.60 (dq, $^2J_{PC}$ = 82.5 Hz, $^3J_{CF}$ = 3.2 Hz, Ni-C), 149.31 (s, Ph-C), 144.55 (s, Py-CH), 143.51 (qd, $^1J_{CF}$ = 357 Hz, $^2J_{PC}$ = 18.4 Hz, $NiCF_3$), 139.83 (m, Ph-CH), 130.83 (d, J_{PC} = 5.9 Hz, Ph-CH), 126.24 (s, Ph-CH), 123.34 (d, J_{PC} = 3.2 Hz, Ph-CH), 112.24 (s, Py-CH), 108.06 (d, J_{PC} = 3.8 Hz, Py-CH), 39.23 [d, $^1J_{PC}$ = 4.9 Hz, $(CH_3)_3$CP], 27.79 [d, $^2J_{PC}$ = 6.5 Hz, $(CH_3)_3$CP]. HRMS (ESI): *m/z* calcd. for $C_{20}H_{25}F_3NNiOP$: 442.1058 [M]$^+$, found 442.1077. UV/Vis (MeCN, nm): λ = 245 (ε = 2.6 × 10^4 L mol^{-1} cm^{-1}), 304 (ε = 5.8 × 10^3 L mol^{-1} cm^{-1}), 331 (ε = 4.5 × 10^3 L mol^{-1} cm^{-1}), 340 (ε = 5.3 × 10^3 L mol^{-1} cm^{-1}), 395 (ε = 1.3 × 10^3 L mol^{-1} cm^{-1}).

Oxidation of 2CH$_3$: A solution of [acetylferrocenium]BF_4 (13 μmol, 4.1 mg) in a mixture of PrCN/MeCN = 3:1 (0.2 mL) was added to a solution of complex **2CH$_3$** (13 μmol, 5.0 mg) in the same solvent (0.2 mL) in the glovebox. 0.2 mL of the reaction mixture was transferred directly to an EPR tube and the sample was frozen in liquid N_2 as fast as possible. Oxidation at low temperature: sample was prepared outside the glovebox at –78 °C and precooled solutions and EPR tube. The sample was directly frozen in liquid N_2.

Synthesis of complex B. To a Schlenk containing complex **2CH$_3$** (10 mg, 0.026 mmol) and $AgBF_4$ (10 mg, 0.052 mmol) was added MeCN (2 mL). The reaction was stirred for 5 minutes after which it was filtered and evaporated to dryness. As the product could not be separated from the nickel-containing by-products, complex **B** was only characterized in situ. ^{1}H NMR (300 MHz, [D3]MeCN, ppm): δ 7.92 (t, J = 7.8 Hz, 1 H), 7.35 (m, 4 H), 7.22 (d, J = 5.2 Hz, 1 H), 7.03 (d, J = 8.0 Hz, 1 H), 2.26 (s, 3 H, Ph-CH_3), 1.25 (d, J = 15.4 Hz, 18 H, $(CH_3)_3$CP). ^{31}P NMR (121 MHz, [D3]MeCN, ppm): δ 139.12 (dd, $^1J_{P\text{-}^{107}Ag}$ = 707 Hz, $^1J_{P\text{-}^{109}Ag}$ = 618 Hz). ^{13}C NMR (75 MHz, [D3]MeCN, ppm): δ 162.30 (s, Py-C), 158.20 (m, Py-C), 142.32 (s, Py-CH), 140.83 (s, Ph-C), 136.56 (s, Ph-C), 131.27 (s, Ph-CH), 130.36 (s, Ph-CH), 129.64 (s, Ph-CH), 126.77 (s, Ph-CH), 112.31 (s, Py-CH), 37.58–36.58 (m, $(CH_3)_3$CP), 27.16 (d, $^1J_{CP}$ = 10.9 Hz, $(CH_3)_3$CP), 20.29 (s, Ph-CH_3). One of the Py-CH signals is obscured by the solvent residual signal. HRMS (CSI): *m/z* calcd. for $C_{22}H_{31}AgN_2OP$: 477.1225 [M]$^+$; found: 477.1248.

Oxidation of $2CF_3$: A solution of [thianthrenium]BF_4 (11 μmol, 3.2 mg) in a mixture of PrCN/MeCN = 3:1 (0.2 mL) was added to a solution of complex **$2CF_3$** (11 μmol, 5.0 mg) in the same solvent (0.2 mL) in the glovebox. 0.2 mL of the reaction mixture was transferred directly to an EPR tube and the sample was frozen in liquid N_2 as fast as possible. Oxidation at low temperature: sample was prepared outside the glovebox at –78 °C and precooled solutions and EPR tube. The sample was directly frozen in liquid N_2.

Oxidation of $2CF_3$ with [thianthrenium]BF_4 in the presence of $AgBF_4$. To a Schlenk containing complex **$2CF_3$** (10 mg, 0.023 mmol), [thianthrenium]BF_4 (7.0 mg, 0.023 mmol) and $AgBF_4$ (4.4 mg, 0.023 mmol) was added MeCN (2 mL). The reaction was stirred for 5 minutes, after which it was filtered and evaporated to dryness. As the product could not be separated from the Ni-containing by-products and thianthrene, the product was only characterized in situ. ^{1}H NMR (300 MHz, [D3]MeCN, ppm): δ 8.00–7.67 (m, 4 H, Py-CH and 3 × Ph-CH), 7.55 (thianthrene and 1 × Ph-CH), 7.33 (m, thianthrene), 7.25 (d, J = 7.38 Hz, Py-CH), 7.12 (d, J = 8.30 Hz, Py-CH), 1.24 (d, J = 15.5 Hz, $(CH_3)_3$CP). ^{31}P NMR (121 MHz, [D3]MeCN, ppm): δ 138.35 (m). ^{19}F NMR (282 MHz, [D3]MeCN, ppm): δ –57.25 (s, Ph-CF_3), –151.76 (s, BF_4). HRMS (CSI): m/z calcd. for $C_{22}H_{28}AgF_3N_2OP$: 531.0942 $[M]^+$; found: 531.0953.

Reduction of $2CH_3$: KC_8 (13 μmol, 1.8 mg) was added to a solution of **$2CH_3$** (13 μmol, 5.0 mg) in THF (0.4 mL) and the reaction was stirred for 90 min at room temp. The reaction mixture was filtered and 0.2 mL was transferred to a capillary inside an EPR tube.

Reduction of $2CF_3$: KC_8 (11 μmol, 1.5 mg) was added to a solution of **$2CF_3$** (11 μmol, 5.0 mg) in THF (0.4 mL) and the reaction was stirred for 90 min at room temp. The reaction mixture was filtered and 0.2 mL was transferred to a capillary inside an EPR tube.

Electrochemistry: All cyclic voltammograms are measured in propionitrile with N(nBu)$_4$$PF_6$ (0.1 M) as the supporting electrolyte. Concentration of the analyte: 6 mM. Working electrode: glassy carbon. Counter electrode: Pt coil. Reference electrode: Ag coil. Scan rate: 100 mV s^{-1}. All redox potentials are referenced to ferrocene/ferrocenium (Fc/Fc^+).

Spectroelectrochemistry: UV/Vis spectra were measured with an optical-transparent-thin-layer electrochemical OTTLE cell. The oxidation and reduction measurements were carried out in propionitrile, MeCN or THF, respectively, with N(nBu)$_4$$NPF_6$ (0.2 M) as the supporting electrolyte. Working electrode: Pt. Counter electrode: Pt. Reference electrode: Ag wire. Scan rate: 0.003 V s^{-1}.

EPR Spectroscopy: Experimental X-band EPR spectra were recorded on a Bruker EMX spectrometer (Bruker BioSpin Rheinstetten) equipped with a He temperature control cryostat system (Oxford Instruments) or a Bruker ELEXSYS500E equipped with a Bruker variable-temperature unit ER 4131 VT (500 to 100 K). Simulations of the EPR spectra were performed by iteration of the anisotropic g-values and line widths using the EPR simulation program W95EPR developed by Prof. Dr. Frank Neese.

Computational Details and EPR Property Calculations: Geometry optimizations were carried out with the Turbomole program package[33] coupled to the PQS Baker optimizer[34] via the BOpt package,[35] at the ri-DFT[36]/BP86[37,38] level. We used Grimmes D3 dispersion corrections (disp3)[39] and the def2-TZVP basis set[40,41] for all atoms, and a small grid (m4). EPR parameters[42,43] were subsequently calculated with the ADF[44–47] program system at the B3LYP/TZ2P level, using the coordinates from the structures optimized in Turbomole as input. ZORA basis sets as supplied with the ADF program were used, employing unrestricted SPINORBIT ZORA COLLINEAR calculations for the SOC corrected HFI-tensors and Zeeman corrected g-tensors. EPR parameters were also calculated with the ORCA program package (version 3.0.3.),[48] again using the coordinates from the structures optimized in Turbomole as input, now employing the B3LYP[49–51] functional and the def2-TZVP basis set.[40,41]

X-ray Crystallography Studies

X-ray intensities were measured on a Bruker D8 Quest Eco diffractometer equipped with a Triumph monochromator (λ = 0.71073 Å) and a CMOS Photon 50 detector at a temperature of 150(2) K. Intensity data were integrated with the Bruker APEX2 software.[52] Absorption correction and scaling was performed with SADABS.[53] The structures were solved using intrinsic phasing with the program SHELXT.[52] Least-squares refinement was performed with SHELXL-2013[54] against F^2 of all reflections. Non-hydrogen atoms were refined with anisotropic displacement parameters. The H atoms were placed at calculated positions using the instructions AFIX 13, AFIX 43 or AFIX 137 with isotropic displacement parameters having values 1.2 or 1.5 times U_{eq} of the attached C atoms.

CCDC 1821417 (for **$2CF_3$**) and 1821418 (for **$2CH_3$**) contain the supplementary crystallographic data for this paper. These data can be obtained free of charge from The Cambridge Crystallographic Data Centre.

For $2CH_3$: $C_{20}H_{29}NNiOP$, Fw = 388.11, T = 150 K, orange plate, 0.197 × 0.221 × 0.431 mm^3, monoclinic, $C2/c$ (no. 15), a = 43.970(3) Å, b = 14.3860(10) Å, c = 24.9872(16) Å, β = 94.791(7)°, V = 15750.5 Å^3, Z = 34, D_x = 1.395 g cm^{-3}, μ = 1.140 mm^{-1}. 221290 Reflections were measured up to a resolution of $(\sin\theta/\lambda)_{max}$ = 0.993 Å^{-1}. 14101 Reflections were unique (R_{int} = 0.1805), of which 9722 were observed [$I > 2\sigma(I)$]. 893 Parameters were refined with no restraints. $R1/wR2$ [$I > 2\sigma(I)$]: 0.0430/0.1084. $R1/wR2$ [all refl.]: 0.0835/0.1331. S = 0.848. Residual electron density found between –0.36 and 0.44 e/Å^3.

For $2CF_3$: $C_{20}H_{25}F_3NNiOP$, Fw = 442.08, T = 150 K, yellow plate, 0.106 × 0.162 × 0.335 mm^3, monoclinic, $P2_12_12_1$ (no. 19), a = 8.1987(10) Å, b = 10.5103(13) Å, c = 23.341(3) Å, V = 2011.31 Å^3, Z = 4, D_x = 1.460 g cm^{-3}, μ = 1.080 mm^{-1}. 40175 Reflections were measured up to a resolution of $(\sin\theta/\lambda)_{max}$ = 0.988 Å^{-1}. 5061 Reflections were unique (R_{int} = 0.0825), of which 3840 were observed [$I > 2\sigma(I)$]; 250 parameters were refined with no restraints. $R1/wR2$ [$I > 2\sigma(I)$]: 0.0428/0.0617. $R1/wR2$ [all refl.]: 0.0824/0.0690. S = 1.028. Residual electron density found between –0.68 and 0.74 e/Å^3.

Complex $2CH_3$: Selected bond lengths [Å] and angles [°] for the other three independent molecules found in the unit cell: Ni2: Ni2–C12B 1.943(4); Ni2–C1B 1.933(4); Ni2–N1B 1.910(3); Ni2–P1B 2.161(1); C1B–Ni2–N1B 83.9(2); C1B–Ni2–C12B 92.4(2); C12B-Ni2–P1B 100.6(1); P1B–Ni2–N1B 83.1(1); C1B–Ni2–P2A 166.9(1). For Ni3: Ni3–C12C 1.957(4); Ni3–C1C 1.939(4); Ni3–N1C 1.916(3); Ni3–P1C 2.173(1); C1C–Ni3–N1C 83.6(2); C1C–Ni3–C12C 93.2(2); C12C–Ni3–P1C 100.2(1); P1C–Ni3–N1C 83.1(1); C1C–Ni3–P1C 166.6(1). For Ni4: Ni4–C12D 1.958(4); Ni4–C1D 1.939(4); Ni4–C1D 1.939(4); Ni4–P1D 2.162(1); C1D–Ni4–N1D 84.0(1); C1D–Ni4–C12D 93.4(2); C12D–Ni4–P1D 99.8(1); P1D–Ni4–N1D 82.88(9); C1D–Ni4–P1D 166.9(1).

Acknowledgments

This research was funded by the European Research Council (ERC) (Starting Grant 279097, *EuReCat*, to J. I. v. d. V.). A. K. and A. S. thank the German Science Foundation Deutsche Forschungsgemeinschaft (DFG) for financial support (KL 1194/15-1). N. V. acknowledges support from PROMI, University of Co-

logne. René Becker and Riccardo Zaffaroni are thanked for their assistance with initial electrochemistry experiments. Prof. František Hartl is thanked for discussions on the spectroelectrochemistry data. Christophe Rebreyend is thanked for help with EPR measurements. Ed Zuidinga is thanked for MS analyses. Prof. Joost N. H. Reek is thanked for general discussions and interest in our work.

Keywords: Nickel · Pincer ligands · Redox chemistry · C–C reductive elimination · Radical ions

[1] a) S. Z. Tasker, E. A. Standley, T. F. Jamison, *Nature* **2014**, *509*, 299–309; b) X. Hu, *Chem. Sci.* **2011**, *2*, 1867–1886.
[2] V. P. Ananikov, *ACS Catal.* **2015**, *5*, 1964–1971.
[3] O. A. Tomashenko, V. V. Grushin, *Chem. Rev.* **2011**, *111*, 4475–4521.
[4] A. G. Algarra, V. V. Grushin, S. A. Macgregor, *Organometallics* **2012**, *31*, 1467–1476.
[5] G. G. Dubinina, W. W. Brennessel, J. L. Miller, D. A. Vicic, *Organometallics* **2008**, *27*, 3933–3938.
[6] J. Jover, F. M. Miloserdov, J. Benet-Buchholz, V. V. Grushin, F. Maseras, *Organometallics* **2014**, *33*, 6531–6543.
[7] A. Klein, A. Kaiser, B. Sarkar, M. Wanner, J. Fiedler, *Eur. J. Inorg. Chem.* **2007**, 965–976.
[8] I. Kieltsch, G. G. Dubinina, C. Hamacher, A. Kaiser, J. Torres-Nieto, J. M. Hutchison, A. Klein, Y. Budnikova, D. A. Vicic, *Organometallics* **2010**, *29*, 1451–1456.
[9] A. Klein, D. A. Vicic, C. Biewer, I. Kieltsch, K. Stirnat, C. Hamacher, *Organometallics* **2012**, *31*, 5334–5341.
[10] V. N. Madhira, P. Ren, O. Vechorkin, X. Hu, D. A. Vicic, *Dalton Trans.* **2012**, *41*, 7915–7919.
[11] Y. Yamaguchi, H. Ichioka, A. Klein, W. W. Brennessel, D. A. Vicic, *Organometallics* **2012**, *31*, 1477–1483.
[12] H. Wang, D. A. Vicic, *Synlett* **2013**, *24*, 1887–1898.
[13] D. G. Morrell, J. K. Kochi, *J. Am. Chem. Soc.* **1975**, *97*, 7262–7270.
[14] a) B. Zheng, F. Tang, J. Luo, J. W. Schultz, N. P. Rath, L. M. Mirica, *J. Am. Chem. Soc.* **2014**, *136*, 6499–6504; b) F. Tang, N. P. Rath, L. M. Mirica, *Chem. Commun.* **2015**, *51*, 3113–3116; c) W. Zhou, J. W. Schultz, N. P. Rath, L. M. Mirica, *J. Am. Chem. Soc.* **2015**, *137*, 7604–7607.
[15] a) Y. Aihara, N. Chatani, *J. Am. Chem. Soc.* **2013**, *135*, 5308–5311; b) Y. Aihara, M. Tobisu, Y. Fukumoto, N. Chatani, *J. Am. Chem. Soc.* **2014**, *136*, 15509–15512.
[16] a) H. M. Omer, P. Liu, *J. Am. Chem. Soc.* **2017**, *139*, 9909–9920; b) J. Xu, L. Qiao, J. Shen, K. Chai, C. Shen, P. Zhang, *Org. Lett.* **2017**, *19*, 5661–5664.
[17] Z.-Y. Xu, Y.-Y. Jiang, H.-Z. Yu, Y. Fu, *Chem. Asian J.* **2015**, *10*, 2479–2483.
[18] a) S. Y. de Boer, T. J. Korstanje, S. R. La Rooij, R. Kox, J. N. H. Reek, J. I. van der Vlugt, *Organometallics* **2017**, *36*, 1541–1549; b) M. Devillard, B. de Bruin, M. A. Siegler, J. I. van der Vlugt, *Chem. Eur. J.* **2017**, *23*, 13628–13832; c) M. Devillard, C. Alvarez Lamsfus, V. Vreeken, L. Maron, J. I. van der Vlugt, *Dalton Trans.* **2016**, *45*, 10989–10998; d) Z. Tang, E. Otten, J. N. H. Reek, J. I. van der Vlugt, B. de Bruin, *Chem. Eur. J.* **2015**, *21*, 12683–12693; e) Y. Gloaguen, W. Jacobs, B. de Bruin, M. Lutz, J. I. van der Vlugt, *Inorg. Chem.* **2013**, *52*, 1682–1684; f) S. Y. de Boer, Y. Gloaguen, J. N. H. Reek, M. Lutz, J. I. van der Vlugt, *Dalton Trans.* **2012**, *41*, 11276–11283; g) S. Y. de Boer, Y. Gloaguen, M. Lutz, J. I. van der Vlugt, *Inorg. Chim. Acta* **2012**, *380*, 336–342; h) R. C. Bauer, Y. Gloaguen, M. Lutz, J. N. H. Reek, B. de Bruin, J. I. van der Vlugt, *Dalton Trans.* **2011**, *40*, 8822–8829; i) J. I. van der Vlugt, E. A. Pidko, R. C. Bauer, Y. Gloaguen, M. K. Rong, M. Lutz, *Chem. Eur. J.* **2011**, *17*, 3850–3854; j) J. I. van der Vlugt, M. A. Siegler, M. Janssen, D. Vogt, A. L. Spek, *Organometallics* **2009**, *28*, 7025–7032; k) J. I. van der Vlugt, M. Lutz, E. A. Pidko, D. Vogt, A. L. Spek, *Dalton Trans.* **2009**, 1016–1023; l) J. I. van der Vlugt, E. A. Pidko, D. Vogt, M. Lutz, A. L. Spek, *Inorg. Chem.* **2009**, *48*, 7513–7515; m) J. I. van der Vlugt, E. A. Pidko, D. Vogt, M. Lutz, A. L. Spek, A. Meetsma, *Inorg. Chem.* **2008**, *47*, 4442–4444.
[19] a) B. Bagh, D. L. J. Broere, V. Sinha, P. T. Kuipers, N. P. van Leest, B. de Bruin, S. Demeshko, M. A. Siegler, J. I. van der Vlugt, *J. Am. Chem. Soc.* **2017**, *139*, 5117–5124; b) V. Vreeken, M. A. Siegler, J. I. van der Vlugt, *Chem. Eur. J.* **2017**, *23*, 5585–5594; c) V. Vreeken, L. Baij, B. de Bruin, M. A. Siegler, J. I. van der Vlugt, *Dalton Trans.* **2017**, *46*, 7145–7149; d) D. L. J. Broere, D. K. Modder, E. Blokker, M. A. Siegler, J. I. van der Vlugt, *Angew. Chem. Int. Ed.* **2016**, *55*, 2406–2410; *Angew. Chem.* **2016**, *128*, 2452; e) D. L. J. Broere, R. Plessius, J. Tory, S. Demeshko, B. de Bruin, M. A. Siegler, F. Hartl, J. I. van der Vlugt, *Chem. Eur. J.* **2016**, *22*, 13965–13975; f) B. Bagh, D. L. J. Broere, M. A. Siegler, J. I. van der Vlugt, *Angew. Chem. Int. Ed.* **2016**, *55*, 8381–8385; *Angew. Chem.* **2016**, *128*, 8521; g) V. Vreeken, D. L. J. Broere, A. C. H. Jans, M. Lankelma, J. N. H. Reek, M. A. Siegler, J. I. van der Vlugt, *Angew. Chem. Int. Ed.* **2016**, *55*, 10042–10046; *Angew. Chem.* **2016**, *128*, 10196; h) D. L. J. Broere, N. P. van Leest, B. de Bruin, J. I. van der Vlugt, *Inorg. Chem.* **2016**, *55*, 8603–8611; i) V. Vreeken, M. Lutz, B. de Bruin, J. N. H. Reek, M. A. Siegler, J. I. van der Vlugt, *Angew. Chem. Int. Ed.* **2015**, *54*, 7055–7059; *Angew. Chem.* **2015**, *127*, 7161; j) D. L. J. Broere, S. Demeshko, B. de Bruin, E. A. Pidko, J. N. H. Reek, M. Lutz, M. A. Siegler, J. I. van der Vlugt, *Chem. Eur. J.* **2015**, *21*, 5879–5886; k) D. L. J. Broere, L. L. Metz, B. de Bruin, J. N. H. Reek, M. A. Siegler, J. I. van der Vlugt, *Angew. Chem. Int. Ed.* **2015**, *54*, 1516–1520; *Angew. Chem.* **2015**, *127*, 1536; l) D. L. J. Broere, B. de Bruin, J. N. H. Reek, M. Lutz, S. Dechert, J. I. van der Vlugt, *J. Am. Chem. Soc.* **2014**, *136*, 11574–11577.
[20] L. S. Jongbloed, B. de Bruin, J. N. H. Reek, M. Lutz, J. I. van der Vlugt, *Chem. Eur. J.* **2015**, *21*, 7297–7305.
[21] L. S. Jongbloed, B. de Bruin, J. N. H. Reek, M. Lutz, J. I. van der Vlugt, *Catal. Sci. Technol.* **2016**, *6*, 1320–1327.
[22] L. S. Jongbloed, D. García-López, R. van Heck, M. A. Siegler, J. J. Carbo, J. I. van der Vlugt, *Inorg. Chem.* **2016**, *55*, 8041–8047.
[23] a) M. B. Watson, N. P. Rath, L. M. Mirica, *J. Am. Chem. Soc.* **2017**, *139*, 35–38; b) N. M. Camasso, A. J. Canty, A. Ariafard, M. S. Sanford, *Organometallics* **2017**, *36*, 4382–4393; c) M. Rovira, S. Roldán-Gómez, V. Martin-Diaconescu, C. J. Whiteoak, A. Company, J. M. Luis, X. Ribas, *Chem. Eur. J.* **2017**, *23*, 11662–11668; d) H. Lee, J. Börgel, T. Ritter, *Angew. Chem. Int. Ed.* **2017**, *56*, 6966–6969; *Angew. Chem.* **2017**, *129*, 7070; e) J. Breitenfeld, J. Ruiz, M. D. Wodrich, X. Hu, *J. Am. Chem. Soc.* **2013**, *135*, 12004–12012; f) M. I. Lipschutz, X. Yang, R. Chatterjee, T. D. Tilley, *J. Am. Chem. Soc.* **2013**, *135*, 15298–15301; g) S. Biswas, D. J. Weix, *J. Am. Chem. Soc.* **2013**, *135*, 16192–16197; h) D. Liu, Y. Li, X. Qi, Y. Lan, A. Lei, *Org. Lett.* **2015**, *17*, 998–1001; i) V. Pandarus, D. Zargarian, *Organometallics* **2007**, *26*, 4321–4334; j) R. A. Gossage, L. A. van de Kuil, G. van Koten, *Acc. Chem. Res.* **1998**, *31*, 423–431.
[24] C.-P. Zhang, H. Wang, A. Klein, C. Biewer, K. Stirnat, Y. Yamaguchi, L. Xu, V. Gomez-Benitez, D. A. Vicic, *J. Am. Chem. Soc.* **2013**, *135*, 8141–8144.
[25] Recent reviews on Nil-chemistry: a) C.-Y. Lin, P. P. Power, *Chem. Soc. Rev.* **2017**, *46*, 5347–5399; b) P. Zimmermann, C. Limberg, *J. Am. Chem. Soc.* **2017**, *139*, 4233–4242.
[26] a) J. T. Ciszewski, D. Y. Mikhaylov, K. V. Holin, M. K. Kadirov, Y. H. Budnikova, O. Sinyashin, D. A. Vicic, *Inorg. Chem.* **2011**, *50*, 8630–8635; b) Y. H. Budnikova, D. A. Vicic, A. Klein, *Inorganics* **2018**, *6*, 1–18.
[27] a) I. Ruppert, K. Schlich, W. Volbach, *Tetrahedron Lett.* **1984**, *25*, 2195–2198; b) G. K. S. Prakash, R. Krishnamurti, G. A. Olah, *J. Am. Chem. Soc.* **1989**, *111*, 393–395; c) G. K. S. Prakash, M. Mandal, *J. Am. Chem. Soc.* **2002**, *124*, 6538–6539. For recent applications of this reagent, see: d) F. Wang, T. Luo, J. Hu, Y. Wang, H. S. Krishnan, P. V. Jog, S. K. Ganesh, G. K. S. Prakash, G. A. Olah, *Angew. Chem. Int. Ed.* **2011**, *50*, 7153–7157; *Angew. Chem.* **2011**, *123*, 7291; e) M. Goswami, B. de Bruin, W. I. Dzik, *Chem. Commun.* **2017**, *53*, 4382–4385.
[28] B. Vabre, P. Petiot, R. Declercq, D. Zargarian, *Organometallics* **2014**, *33*, 5173–5184.
[29] F. Hung-Low, K. K. Klausmeyer, *Inorg. Chim. Acta* **2008**, *361*, 1298–1310.
[30] X. Wang, L. Truesdale, J.-Q. Yu, *J. Am. Chem. Soc.* **2010**, *132*, 3648–3649.
[31] A. Klein, B. Rausch, A. Kaiser, N. Vogt, *J. Organomet. Chem.* **2014**, *774*, 86–93.
[32] a) W. Kaim, *Eur. J. Inorg. Chem.* **2012**, 343–348; b) J. I. van der Vlugt, *Eur. J. Inorg. Chem.* **2012**, 363–375; c) K. G. Caulton, *Eur. J. Inorg. Chem.* **2012**, 435–443; d) V. Lyaskovskyy, B. de Bruin, *ACS Catal.* **2012**, *2*, 270–279; e) D. L. J. Broere, R. Plessius, J. I. van der Vlugt, *Chem. Soc. Rev.* **2015**, *44*, 6886–6915.
[33] R. Ahlrichs, *Turbomole Version 6.5*, Theoretical Chemistry Group, University of Karlsruhe, **2013**.

[34] *PQS version 2.4*, Parallel Quantum Solutions, Fayetteville, Arkansas (USA), **2001**. The Baker optimizer is available separately from PQS upon request: I. Baker, *J. Comput. Chem.* **1986**, *33*, 8822–8824.
[35] P. H. Budzelaar, *J. Comput. Chem.* **2007**, *28*, 2226–2236.
[36] M. Sierka, A. Hogekamp, R. Ahlrichs, *J. Chem. Phys.* **2003**, *118*, 9136–9148.
[37] A. D. Becke, *Phys. Rev. A* **1988**, *38*, 3098–3100.
[38] J. P. Perdew, *Phys. Rev. B* **1986**, *33*, 8822–8824.
[39] S. Grimme, J. Antony, S. Ehrlich, H. Krieg, *J. Chem. Phys.* **2010**, *132*, 154104–154119.
[40] F. Weigend, M. Häser, H. Patzelt, R. Ahlrichs, *Chem. Phys. Lett.* **1998**, *294*, 143–152.
[41] F. Weigend, R. Ahlrichs, *Phys. Chem. Chem. Phys.* **2005**, *7*, 3297–3305.
[42] E. van Lenthe, A. D. van der Avoird, P. E. S. Wormer, *J. Chem. Phys.* **1998**, *108*, 4783–4796.
[43] E. van Lenthe, P. E. S. Wormer, A. D. van der Avoird, *J. Chem. Phys.* **1997**, *107*, 2488–2498.
[44] E. J. Baerends, D. E. Ellis, P. Ros, *Chem. Phys.* **1973**, *2*, 41–51.
[45] L. Versluis, T. Ziegler, *J. Chem. Phys.* **1988**, *88*, 322–328.
[46] G. Te Velde, E. J. Baerends, *J. Comput. Phys.* **1992**, *99*, 84–98.
[47] C. Fonseca Guerra, J. G. Snijders, G. Te Velde, E. Baerends, *J. Theor. Chem. Acc.* **1998**, *99*, 391–403.
[48] F. Neese, *Comp. Mol. Sci.* **2012**, *2*, 73–78.
[49] C. Lee, W. Yang, R. G. Parr, *Phys. Rev. B* **1988**, *37*, 785–789.
[50] A. D. Becke, *J. Chem. Phys.* **1993**, *98*, 5648–5652.
[51] A. D. Becke, *J. Chem. Phys.* **1993**, *98*, 1372–1377.
[52] Bruker, *APEX2* software, Madison WI, USA, **2014**.
[53] G. M. Sheldrick, *SADABS*, Universität Göttingen, Germany, **2008**.
[54] G. M. Sheldrick, *SHELXL**2013***, University of Göttingen, Germany, **2013**.

Received: February 5, 2018